Aircraft Noise Emission Model Accounting for Aircraft Flight Parameters

C. Zellmann,* B. Schäffer,† and J. M. Wunderli†
Empa, 8600 Dübendorf, Switzerland
U. Isermann‡
DLR, German Aerospace Center, 37073 Göttingen, Germany
and
C. O. Paschereit§
Berlin University of Technology, 10623 Berlin, Germany

DOI: 10.2514/1.C034275

Today's aircraft noise calculation programs either use simple sound source descriptions with few input parameters or highly sophisticated models with input parameters, which are difficult to obtain. To fill the gap between these two approaches, an aircraft noise emission model based on regression of measured noise with aircraft flight parameters is presented. To find a reasonable compromise between the degree of detail and number of required flight parameters, an extensive data exploration was conducted. The most relevant parameters were incorporated in two multiple linear regression models, one for airframe and one for engine noise sources. An iterative method allowed fitting both regression models to aircraft flyover measurements. In total, aircraft noise emission models for 19 aircraft types were established, which underlines the general applicability of the modeling approach to turbofan-powered aircraft. Example comparisons between measurements and model predictions for two aircraft types revealed that the model accurately reproduces directivity and spectra for different flight configurations. In addition, it is suitable for the assessment and optimization of noise abatement procedures.

I. Introduction

AIRCRAFT noise calculations are essential for land-use planning and management worldwide. Furthermore, they allow assessment and optimization of noise abatement procedures for a quieter environment. Both topics are important elements of the Balanced Approach to Aircraft Noise by the International Civil Aviation Organization (ICAO) [1]. The former element is well established by best practice programs, which are developed to calculate the sound level at the receiver. For this purpose, international harmonized methods such as ICAO Doc. 9911 [2], ECAC Doc. 29, and national models as the AzB [3,4] in Germany or FLULA2 [5] in Switzerland are applied. For the latter element, more sophisticated models, which describe the sound emission and propagation separately, are needed to accurately calculate the noise of single-flight procedures [6]. ANOPP [7], SIMUL [8], and PANAM [9] are current programs that fulfill this requirement.

However, aircraft noise prediction models for legal compliance as well as sophisticated semi-empirical models for scientific purposes have their limitations in the assessment of noise abatement procedures. For instance, the influence of aircraft speed or configuration on sound emission is not accounted for in legal compliance models. In addition, the acoustical description is simplified to generalized spectral classes (Doc. 9911/Doc. 29) or fixed to a standard atmosphere (FLULA2), which further increase the model uncertainty. These shortcomings are no issue for aircraft noise emission models such as ANOPP, SIMUL, or PANAM, which predict spectra and directivity for each source on a high level of detail. However, they require very detailed input data of geometry as well as physical flight parameters (e.g., primary jet speed or airflow mass) for accurate predictions. Another drawback is the limited accessibility of these programs to other users and a database limited to a small number of aircraft [10].

The present work introduces an aircraft noise emission model that overcomes many of these limitations. First, the model is based on backpropagated flyover measurements, which are separated into airframe and engine noise. The separation of the data set is part of an iterative process to establish the regression models. Therefore, no complex measurements with microphone arrays are necessary, and the model can be applied to any turbofan-powered aircraft type. Second, the model describes the sound emission in 1/3-octave bands, accounting for directivity and major flight parameters.

Section II gives an overview of the input data and its processing. The data exploration and separation to airframe and engine noise are described in Sec. III. The regression models are presented in Sec. IV. Finally, example results and comparisons to measurements for two aircraft types with different underlying data sets are presented and discussed.

II. Input Data

A. Measurements and Data Sources

Acoustical overfly measurements of regular air traffic were performed around Zurich Airport. To cover a wide range of typical flight configurations (i.e., flight parameters and aeroplane configuration [2]), microphones were placed in the vicinity of the airport but also farther away at varying distances, up to 20 km. Figure 1 depicts the measurement setup in the far range covering approaches from the south and two departure routes, covering wide- and narrow-body aircraft. The microphone locations for departures were selected to cover flight configurations after cutback, during acceleration, and continuous climb in clean configuration. For approach, the microphone locations were distributed along the glide path where the aircraft deploy the high-lift devices and landing gear to prepare for final approach. The equipment at all locations operated

Received 27 October 2016; revision received 6 July 2017; accepted for publication 9 July 2017; published online 28 August 2017.

*Ph.D. Candidate, Swiss Federal Laboratories for Materials Science and Technology, Laboratory for Acoustics/Noise Control, Überlandstr. 129.

†Research Engineer, Swiss Federal Laboratories for Materials Science and Technology, Laboratory for Acoustics/Noise Control, Überlandstr. 129.

‡Research Engineer, Institute of Aerodynamics and Flow Technology, Bunsenstr. 10.

§Professor, Institute of Fluid Dynamics and Technical Acoustics, Müller-Breslau-Strasse 8. Senior Member AIAA.

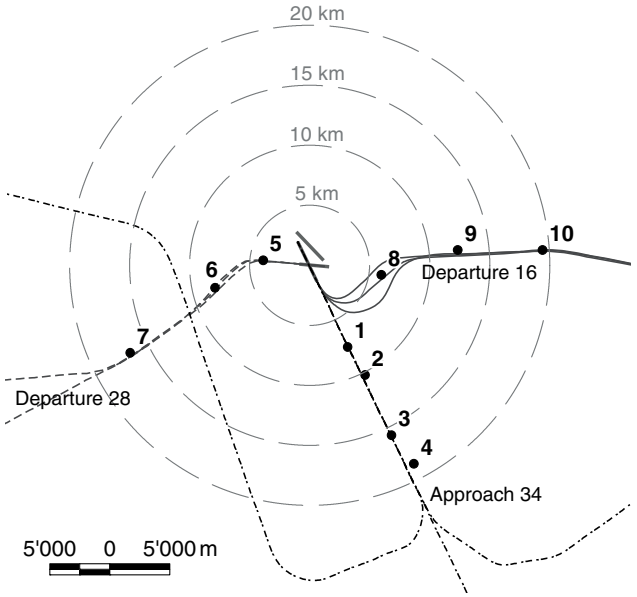

Fig. 1 Measurement setup in the far range of Zurich airport (Microphone locations 1–10).

autonomously and was equipped with weather-protected omnidirectional free-field microphones at a height of 10 m.

Measurements in the close vicinity to the airport, within 2.5 km distance from liftoff or touchdown, provided data for the final approach as well as for initial climb over a wide range of radiation angles (see [11]). For each of the three measured runway directions in the close range, eight omnidirectional free-field microphones were installed at a height of 4 m.

An optical tracking system and a multilateration system delivered positional data with high accuracy in the close range of the airport. In the far range, where the accuracy of radar data is sufficient, the latter was used. In addition, GPS-based flight paths were available from flight data recorder (FDR) data, which are the logged sensor data from the operations of the local carrier Swiss International Air Lines. The FDR data further provided information such as airspeed, engine performance parameters, aircraft orientation, configuration of the airframe, or ambient conditions. For aircraft types without available FDR data, the rotational speed of the engine $N1$ was extracted from the acoustical measurements by detecting the blade-passing frequency (BPF) from the spectrogram [12]. In total, data of six aircraft types based on FDR data and 13 grouped aircraft types based on $N1$ determination were available for data processing (Table A1, Appendix). Because the aircraft types with FDR data from the local carrier operated frequently, 161 to 673 flights per aircraft type were collected during the measurements. For other aircraft types without FDR data, 27 to 334 flights were measured.

B. Data Processing

Figure 2 depicts the data processing applied to backpropagate the measurements and to establish the input data set for the aircraft noise emission model. The acoustic wave files were analyzed with a constant time interval of 50 ms and filtered to 24 1/3-octave bands with midfrequencies from 25 Hz to 5 kHz to obtain the sound pressure levels $L_{p,50\,\mathrm{ms}}(f)$. The low-frequency boundary was chosen to cover the low-frequency noise from the jet. Frequencies above 5 kHz were omitted because they are quickly attenuated over the normally relatively large distances between aircraft and receiver.

To prevent backpropagation of background noise, only the part of the level-time-history (separately for each 1/3-octave band) being 6 dB above the minimum level before and after the event was selected for the analysis. In addition, events with nonaircraft noise contamination were rejected. To backpropagate the measurements, the sound propagation model sonX, which was developed for train and shooting noise [13–16], was modified for aircraft noise calculation requirements of high sources and used to calculate the corresponding

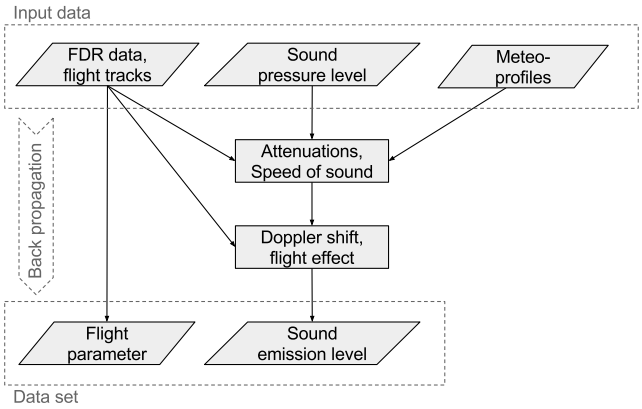

Fig. 2 Flowchart of the data processing.

attenuations and the speed of sound for each source–receiver combination. In sonX, the geometrical divergence, atmospheric absorption, ground effect, foliage attenuation, and the influence of vertical gradients of wind, temperature, and relative humidity are accounted for. For each flight, individual meteorological profiles from the numerical weather prediction model COSMO-2 were used to reproduce the real atmospheric conditions as precisely as possible [17]. The atmospheric absorption coefficient was calculated for different altitudes with a maximum step size of 100 m. Source positions and flight parameters were synchronized with the acoustical data and corrected for the time delay of the sound propagated through the atmosphere.

Effects due to the motion of the source were corrected by applying a frequency shift and a level amplification. In Eq. (1), the Doppler factor (DF) is defined in dependency of the relative aircraft Mach number (i.e., the speed of movement of the source toward the receiver), where θ is the radiation angle between the flight path and the vector from source to receiver:

$$\mathrm{DF} = 1 - Ma \cdot \cos(\theta) \tag{1}$$

Flight effects, as classified by Stone [18] for sound sources that move with the aircraft, consist of the kinematic effect corresponding to the motion of the source relative to the receiver as well as the dynamic effect corresponding to the motion of the source relative to the propagation medium. Combining both effects leads to the level amplification ΔL_{FE} defined in Eq. (2), which was experimentally confirmed by [19]:

$$\Delta L_{\mathrm{FE}} = 40 \cdot \log_{10}\mathrm{DF}^{-1} \tag{2}$$

Equation (3) summarizes the backpropagation calculation to obtain the sound emission levels $L_{\mathrm{em}}(f)$ for each 1/3-octave band. In this paper, the sound emission level $L_{\mathrm{em}}(f)$ is defined as a sound power level $L_W(f)$ but with directivity $D(f)$ already included. This description is necessary because only the lower half-sphere of the aircraft can be measured from the ground:

$$\begin{aligned} L_{\mathrm{em}}(f) &= L_W(f) + D(f) - \Delta L_{\mathrm{FE}} \\ &= L_{p,50\,\mathrm{ms}}(f) + \sum A(f) - \Delta L_{\mathrm{FE}} \end{aligned} \tag{3}$$

The backpropagation from each receiver to the source positions was performed based on the measured sound pressure levels $L_{p,50\,\mathrm{ms}}(f)$, which were corrected for the sum of the propagation attenuation $A(f)$ and the flight effect ΔL_{FE}. Each $L_{\mathrm{em}}(f)$ corresponds to a certain angle combination (θ, φ) on the directivity pattern. Because of the number of flights per aircraft type and the variations of their flight paths, each receiver contributes data points to a certain area, as presented in [11]. In line with the definition of the sound power level with a reference radius of 1 m, the geometrical divergence includes the conversion $\sum A(f)$ constant $\log_{10}(4\pi)$.

The Doppler shift is defined by the frequency ratio of source and receiver, which equals the inverse Doppler factor. For 1/3-octave bands, the Doppler shift was implemented under the assumption of equally distributed energy over each band. It was applied after performing the backpropagation to the source according to Eq. (3).

C. Resulting Data Set

A data set was prepared for all events of each individual combination of aircraft type and engine type as the basis for the model development. The level of detail describing the aircraft was limited to major aircraft and engine types; thus, optional equipment such as winglets or dual annular combustors was not differentiated. For instance, the A320 family was divided into its types A319, A320, and A321, which mainly differ in length and maximum takeoff weight. For every type of this family, different engine options, such as the CFM56 or V2500, are available, which implies six possible data sets if all combinations were measured.

Each data set consisted of 24 subsets for the evaluated 1/3-octave bands with midfrequencies from 25 Hz to 5 kHz. A subset included the corresponding emission levels L_{em} in decibels from Eq. (3), calculated radiation angles θ, φ in degrees, flight parameters such as the rotational speed of the engines $N1$ in %, aircraft Mach number Ma, and the atmospheric parameters pressure p in pascals, temperature T in degrees Celsius, density ρ in kilograms per cubic meter, and speed of sound c in meters per second. If FDR data were available, also the angle of attack, sideslip, and the setting of the configuration were available. The aircraft Mach number could be matched to the true airspeed (with respect to the moving air) of the aircraft, but for consistency, it is related to the flight-path velocity (with respect to the ground), which was available for all aircraft.

In addition, identification numbers for the event and microphone were appended to each data point (line) for traceability during model development. An event with a flight segment of 60 s added 1200 data points per microphone to the data set. For all flights and measurement locations, the subsets (data for each 1/3-octave band) added up to one to two million data points.

III. Data Exploration and Separation

The aircraft noise emission model is based on multiple linear regression. This method allows for identifying effects of different explanatory variables in great detail. The model was established as follows. In the first step, outliers were removed from the data sets (Sec. III.A). Then, the variables for the models were selected (Sec. III.B). Thereafter, a process to separate the data set to airframe and engine noise was applied (Sec. III.C). This separation of the two main noise sources is beneficial because each source can be described more precisely. For instance, the two models may include different variables or may account for different relations with the same explanatory variable.

Data processing, data analysis, and fitting of the aircraft noise emission models (Sec. IV) were conducted with Matlab 2014b. The models were fitted with the Statistical Toolbox via the command fitlm, which uses an ordinary least-squares fit and allows for individual weighting of the data points.

A. Detection of Outliers

Outliers were removed by an adaptive outlier detection method of Filzmoser et al. [20]. This method uses the robust Mahalanobis distance to automatically detect outliers. An advantage of the method is the adjusted threshold, which adapts to the sample size. If the data set originates from a multivariate normal distribution, no outliers would be detected, in contrast to a fixed threshold.

B. Data Exploration

In this section, the available variables of the presented data set are discussed by means of exploratory analysis and knowledge from literature. The findings are used to select the most important explanatory variables for the statistical model, which will be presented in Sec. IV. Also, variables are rejected if they correlate with other variables to ensure reliable model coefficients. Finally, to comply with the linearity of the statistical model, the relationships of the variables to L_{em} are revealed.

1. *Rotational Speed of the Compressor*

For many engines, $N1$ is the control parameter of the power setting. In contrast to the thrust or jet velocity of the engine, it is a directly measurable parameter. The jet velocity, which is the main physical cause for jet noise (see for example Lighthill [21]) correlates with $N1$. Thus, for frequencies below 1 kHz, where jet mixing noise is dominant [22,23], $N1$ can be used as a substitute for the jet velocity. In addition, also the BPF as well as the fan broadband noise with a center frequency of 2.5 times the BPF [24] are directly connected to $N1$. For most engine types, the BPF and thus the broadband noise can be found above 1 kHz; hence, $N1$ is a reasonable explanatory variable for the whole engine spectra.

An engine run-up test of an A330-300 with the TRENT772B was evaluated to establish the functional relation between sound pressure level and $N1$ for each 1/3-octave band because no such relation was known to the authors. The run-up test was executed by Swiss International Air Lines and the measurements done by Empa and Zurich airport; permission for the data was kindly granted. Unweighted sound pressure levels L_p were measured at four microphone locations at a radius of 170 m around the aircraft. During the run-up test, six different engine loads from idle power to the highest possible engine pressure ratio on ground were driven. A full cycle was completed after stepwise reducing the engine load to idle power again. After two cycles, two to four mean L_p were available for each time interval with constant $N1$ (symbols in Fig. 3). A regression model was fitted for each direction with a second-order polynomial fit for $N1$, where 0 deg corresponds to the aircraft's nose.

According to Figs. 3a and 3b, which show two example 1/3-octave bands, the functional relation depends on frequency and direction. For 31.5 Hz, the fit is slightly parabolic to the front and almost linear to the rear of the aircraft. In addition, the slope increases to the rear. For some frequencies such as 2 kHz, the curvature of the quadratic fit is negative (50 to 120 deg) as well as positive (15 deg). For frequencies in between, which are not shown here, the relations are very similar, with mainly linear or slightly quadratic behavior (negative curvature). Thus, a second-order polynomial approach in dependency of the polar angle θ adequately represents the relation between L_p and $N1$ for each 1/3-octave band.

In general, the turbofan engines of today's civil aircraft are very similar, and the mechanisms of sound generation are the same. Therefore, it is assumed that the second-order polynomial approach is also valid for other turbofan engines. This assumption was confirmed with the backpropagated data set shown in Fig. 4 for the Airbus A320 (CFM56-5B) at 2 kHz, which shows the same trends for the L_{em} vs $N1$ (negative as well as positive curvature).

2. *Aircraft Mach Number*

The aircraft Mach number $Ma = U/c$ is chosen to take the speed-dependent sound sources into account. It represents the ratio of the mean flow speed U at the source, here simplified to the flight path velocity (see Sec. II.C), as well as the local speed of sound c in a single, dimensionless variable. Furthermore, the aircraft Mach number is an aerodynamic characteristic that is interpreted as a compressible flow condition and therefore ensures comparable flow phenomena.

The dependency of the sound emission of airframe noise sources to Mach number is provided by the aeroacoustic analogy of Lighthill [21]. The generation of sound from the fluctuating fluid is described by the classical wave equation, which is extended by three basic source terms: monopole, dipole, and quadrupole. The theoretical free-field solutions in Eq. (4) from Ribner [25] reveal that the sound power W is proportional to the air density ρ, a characteristic dimension of the source D, the mean flow speed U, and the Mach number Ma. The exponent l depends on the source term (monopole $l = 1$, dipole $l = 3$, quadrupole $l = 5$):

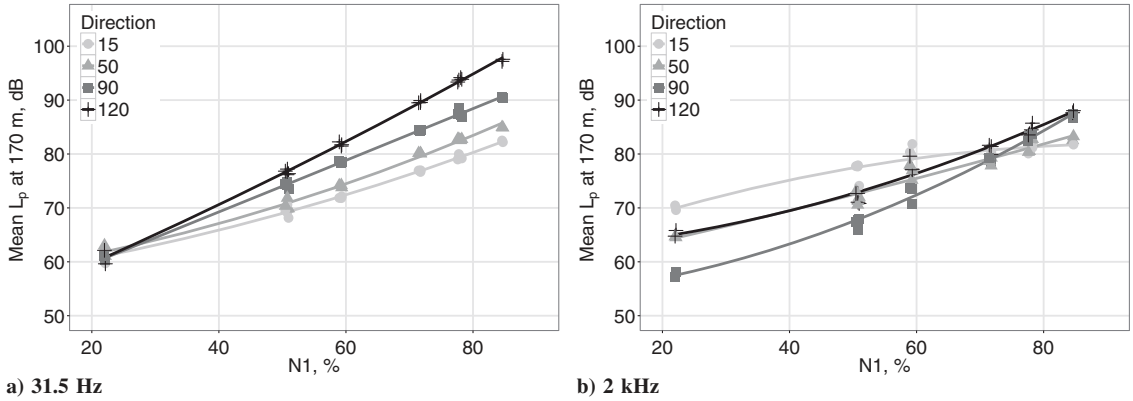

a) 31.5 Hz b) 2 kHz

Fig. 3 Engine run-up test results of the A330-300 (TRENT772B) for two example 1/3-octave bands (aircraft nose represents 0 deg).

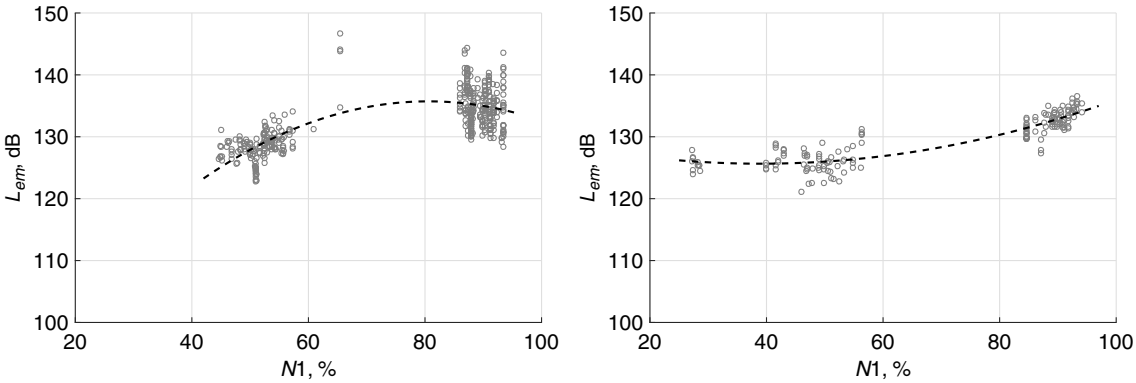

a) $N1$-behavior at $\theta = 30°$, $R^2 = 0.54$ b) $N1$-behavior at $\theta = 120°$, $R^2 = 0.81$

Fig. 4 Influence of $N1$ on L_{em} of the A320 with CFM56-5B for 2 kHz. The data set is presented for $0.2 < Ma < 0.24$.

$$W \propto \rho D^2 U^3 Ma^l \tag{4}$$

To derive the relation for the sound power level L_W, the base-10 logarithm is applied [Eq. (5)]. The units of the parameters are therefore normalized by ρ_0, D_0, U_0:

$$L_W \propto 10\log_{10}\left(\frac{\rho}{\rho_0}\cdot\frac{D^2}{D_0^2}\right) + 10\log_{10}\left(\frac{U^3}{U_0^3}\right) + 10\log_{10}(Ma^l) \tag{5}$$

Equation (5) is applied to the L_{em}, which is proportional to L_W as defined in Eq. (3). In the linear regression model, the implementation of U and Mach number is problematic because these parameters are highly correlated (multicollinearity). The multicollinearity can have strong effects on the estimates of the regression coefficients. Even if the model equation may still be useful in its known intervals, the individual effects of the variables may be poorly estimated and would lead to incorrect extrapolations. To prevent for multicollinearity, instead of $\log_{10}(U)$, only $\log_{10}(Ma)$ is accounted for. Neglecting $\log_{10}(U)$ does not limit the regression model; it is just not possible to separate the effect of highly correlated variables by means of multiple linear regression.

Also engine noise is affected by the aircraft Mach number due to the reduced relative jet speed. For instance, during takeoff roll at ground, which is the flight segment of acceleration on the runway, a linear relation to the speed of the surrounding airflow was found by [26]. The sound pressure level of the jet in the far field decreases with increasing flow speed U, which was confirmed experimentally by [27].

Figure 5 depicts the dependency of L_{em} on Mach number at 250 Hz for typical flight configurations of takeoff with high power (Fig. 5a) and approach with idle power (Fig. 5b). For the climb segment after liftoff, where engine noise dominates, a linear regression shows a slight decrease of L_{em} with Mach number. The coefficient of determination of the regression is only small ($R^2 = 0.1$) because the effect of the aircraft Mach number is small, and the variation of the data is large due to turbulence and uncertainty of the backpropagation. The decrease of L_{em} is explained with the same physical effect that occurs during takeoff roll at ground; the jet noise is reduced with increasing speed of the surrounding airflow. For the takeoff roll, no data were measured, but with the theoretical support from [26,27], a linear extrapolation seems reasonable. Therefore, the relation $L_{em} \propto Ma$ is used for the development of the engine noise model.

In contrast, airframe noise is likely to dominate for the approach in Fig. 5b, where the engines are running in idle power. The coefficient of determination of a logarithmic regression is low with $R^2 = 0.29$ because the variation of the backpropagated $L_{p,50\,\mathrm{ms}}$ is large. For the available data points, a linear relation between L_{em} and Mach number would be as reasonable as a logarithmic relation. However, the theoretical considerations from Eq. (5) suggest a logarithmic behavior, whereas a linear relation would not represent the physics of airframe noise and thus overestimate levels for small and large aircraft Mach numbers. Hence, for the development of the airframe model, the relation $L_{em} \propto \log_{10}(Ma)$ is used.

3. *Atmospheric Parameters*

The effect of the air density is included in the airframe model to account for the generalized aeroacoustic theory in Eq. (5). The air density highly correlates with the air pressure p and temperature T, which were excluded from the regression model to prevent multicollinearity of the variables. Multicollinearity was checked by means of the variance inflation factor (VIF), which was determined for each possible variable [28]. After rejecting p and T, no strong multicollinearity was left. Nevertheless, it was decided to also reject the speed of sound c because this variable is already accounted for with the Mach number. In fact, with the rejection of c, the VIFs of listing of variables, please use Ma and ρ further decreased.

Therefore, ρ is chosen as the only atmospheric variable for the statistical model. Given Eq. (5), again the base-10 logarithm needs to

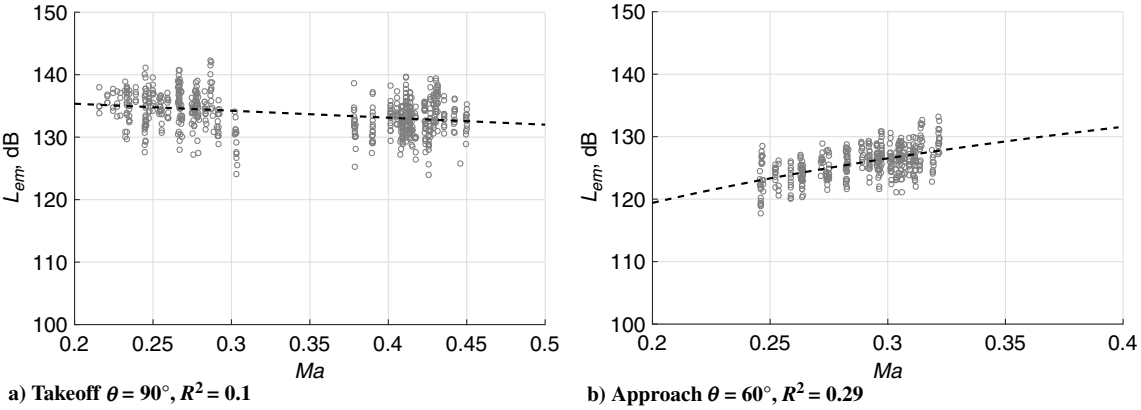

a) Takeoff $\theta = 90°$, $R^2 = 0.1$ **b) Approach $\theta = 60°$, $R^2 = 0.29$**

Fig. 5 Influence of the Mach number on the sound emission level of the A320 at a) takeoff, and b) approach at 250 Hz. The dashed line is a linear regression in Fig. 5a and a logarithmic regression in Fig. 5b.

be applied on ρ. Such transformation guarantees linear behavior with respect to the coefficients of the airframe model.

4. Radiation Angles

The sound emission of an aircraft has a directivity that is best described with spherical coordinates. Particularly the longitudinal radiation, represented by the polar angle θ, strongly changes with aircraft type, 1/3-octave band, and power setting, as shown in Fig. 3 The lateral radiation, represented by the azimuth angle φ, is also taken into account in dependency of aircraft type, 1/3-octave band, and power setting. Lateral directivity can lead to level differences up to 3 dB over φ [29]. Additionally, the lateral directivity in [29] strongly differed from the generalized corrections proposed in Doc. 29 [30].

A Fourier series of second order was chosen to describe the longitudinal directivity. It is a simple mathematical approach that can be implemented to the regression model to reproduce different directivity patterns. Other possible approaches such as spherical hemispheres are also possible descriptions for the directivity, but they are less straightforward to implement in the regression model. During the model development, a higher-order Fourier series was also tested but resulted in problematic slopes at the borders, where less data are available. Particularly for conditions far away from the receivers, the directivity at high frequencies was critical. The lateral directivity is modeled with a half-range Fourier series of second order to simplify the number of terms and also to prevent problematic slopes in areas with low data coverage.

5. Aeroplane Configuration

The aeroplane configuration of the aircraft is accounted for by three explanatory variables: the position of the landing gear (retracted 0, deployed 1), the position of the flap handle (0 to 4, fix combinations of slat and flap deflection), and the deployment of the speedbrakes (inactive: 0, active: 1). These flight parameters were provided by the FDR data. With the measurement of regular air traffic, the data were naturally not balanced, and it was not possible to gain data for all combinations of configurations.

Figure 6 shows the effect of the landing gear on the sound emission level of the A320. The data points are measurements for idle approach conditions with landing gear retracted or deployed. Each data set is fitted with a simple logarithmic regression to show the influence of the landing gear. Measured data and the regression lines show a considerable effect on the sound emission level when the landing gear is deployed. In Fig. 6a, a slightly larger slope of the regression with deployed landing gear can be found. For low Mach number, the emission levels are similar, but for large Mach number of 0.3, the level difference is 2.6 dB. At 2 kHz in Fig. 6b, the effect of the landing gear on the Mach number dependency of the sound generation is much stronger. At $Ma = 0.3$, the difference is already 6 dB. These findings show that the landing gear is not only to be considered as an explanatory variable but also in dependency of the aircraft Mach number.

The setting of the high-lift devices highly correlate to different intervals of aircraft Mach numbers due to the procedures and structural limits, as shown in Fig. 7 In addition, the flap handle position 1 for departures corresponds to a different deflection angle of the flaps than for approach (10 deg instead of 0 deg). Although difficult to account for, the influence of the aircraft configuration is of interest and therefore accounted for with a specific model structure as described in Sec. IV.B.

6. Other Variables

Further variables were considered but rejected during model development due to insignificance or practical reasons. In particular, the angle of attack and angle of sideslip, which are available from FDR data, were excluded because no correlations were found with

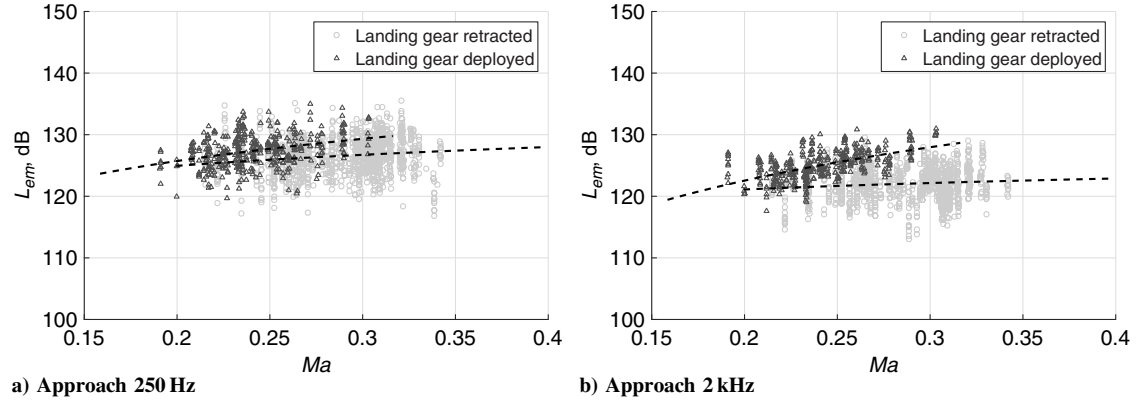

a) Approach 250 Hz **b) Approach 2 kHz**

Fig. 6 Influence of landing gear on the sound emission of the A320 at idle approach for a) 250 Hz, and b) 2 kHz.

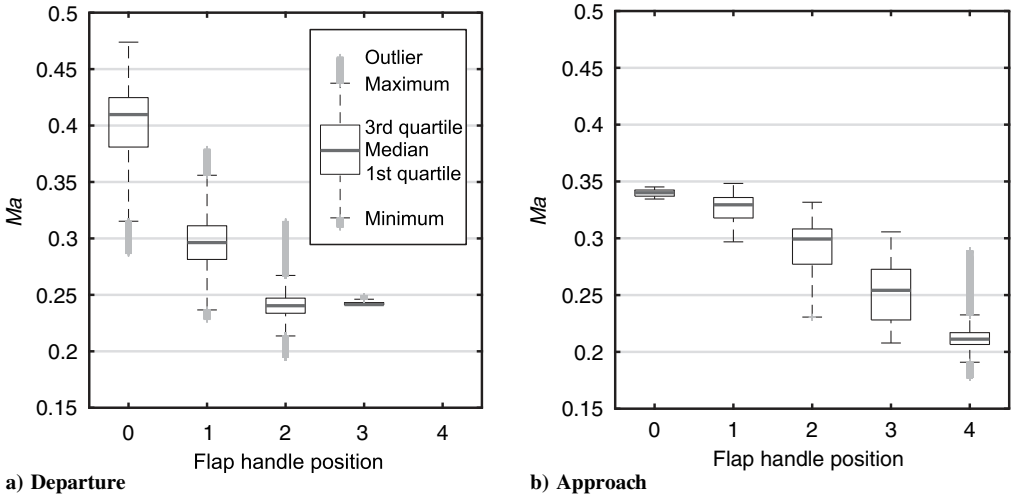

Fig. 7 Variation in the distribution of the aircraft Mach number depending on the flap handle position of the A320.

the emission level. The rejection of both angles is also reasonable because they are usually not available for noise predictions.

C. Data Separation

In Fig. 8, the process of separating the total noise emission levels into airframe and engine noise is shown. In step 1, the data set is separated into two subsets: subset one contains data for the engines running in idle (i.e., only approach conditions), and subset two contains all other data from approach and departure with engines on load. It is assumed that airframe noise is dominating the total L_{em} for subset one.

The limit for the separation with $N1 = 40\%$ was determined by engineering judgment and from data plots of L_{em} versus $N1$ (Fig. 9). With a higher limit (e.g., 50%), the contribution of the engines increases and more likely results in overestimating the contribution of airframe noise. With a lower limit (e.g., 30%), the number of observations would substantially decrease and would prevent from establishing reliable model coefficients. Although the separation limit thus seems feasible, the iterative process of the data separation further refines the initial ratio (step 3) between airframe and engine noise.

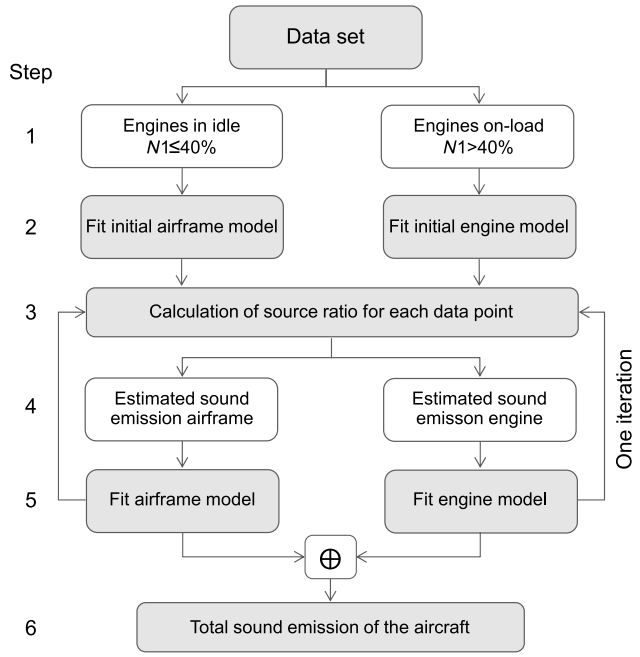

Fig. 8 Process to separate the data set to airframe and engine noise and to establish the regression models. The process is repeated for each 1/3-octave band.

In step 2, an initial airframe and an initial engine model are fitted to their corresponding data sets to reveal the main effects for each source. The initial models are only minor modifications of the models presented in Sec. IV. For the initial airframe model, the variable Proc is inapplicable because the data set includes only approach situations. The initial engine model omits the quadratic relation of $N1^2$ to prevent negative slopes for the extrapolation of $N1$ below 40%. Using the predicted initial airframe ($\hat{L}^i_{\mathrm{em,afm}}$) and engine ($\hat{L}^i_{\mathrm{em,eng}}$) sound emission levels, a source ratio can be calculated for each data point in the original data set (step 3). The ratio q^i [Eq. (6)] is defined as the predicted sound emission of the engine divided by the sum of predicted engine and airframe emission:

$$q^i(f) = \frac{10^{0.1\hat{L}^i_{\mathrm{em,eng}}(f)}}{10^{0.1\hat{L}^i_{\mathrm{em,eng}}(f)} + 10^{0.1\hat{L}^i_{\mathrm{em,afm}}(f)}} \tag{6}$$

A ratio q^i of 0 means that only airframe noise contributes to the total sound emission, and 1 corresponds to engine sound emission only. Note that all predictions from these models are marked by a hat to distinguish from input data; the superscript i indicates that the initial models are used.

Because the initial models were established based on a limited data range (namely, the initial airframe model on approaches with Mach number smaller than 0.35 and the initial engine model on departures with Mach number up to 0.45), the models have to be extrapolated to predict $\hat{L}^i_{\mathrm{em,afm}}$ for each data point on the whole data set. Nevertheless, because the extrapolation for the aircraft Mach number is based on physical knowledge (see Sec. III.B), it allows for a plausible first estimation.

Based on the ratio q^i, two separated data sets, both including all measurements for approach and departure, were created for each 1/3-octave band (step 4). One represents the sound emission of the engines $L^i_{\mathrm{em,eng}}$ and the other the sound emission level of the airframe $L^i_{\mathrm{em,afm}}$:

$$L^i_{\mathrm{em,eng}}(f) = L_{\mathrm{em}}(f) + 10\log_{10}(q^i(f)) \tag{7}$$

$$L^i_{\mathrm{em,afm}}(f) = L_{\mathrm{em}}(f) + 10\log_{10}\left(1 - q^i(f)\right) \tag{8}$$

Figure 9 compares both data sets to the original L_{em}. The airframe levels are dominating for $N1 < 40\%$, which is the implication of the assumption in step 1, whereas they are approximately 20 dB lower than the total levels for departures. In contrast, the engine levels (bottom right) are dominant for departures and lose influence at lower $N1$. In total, by adding the individual levels of both data sets energetically, the original data set can be reconstructed.

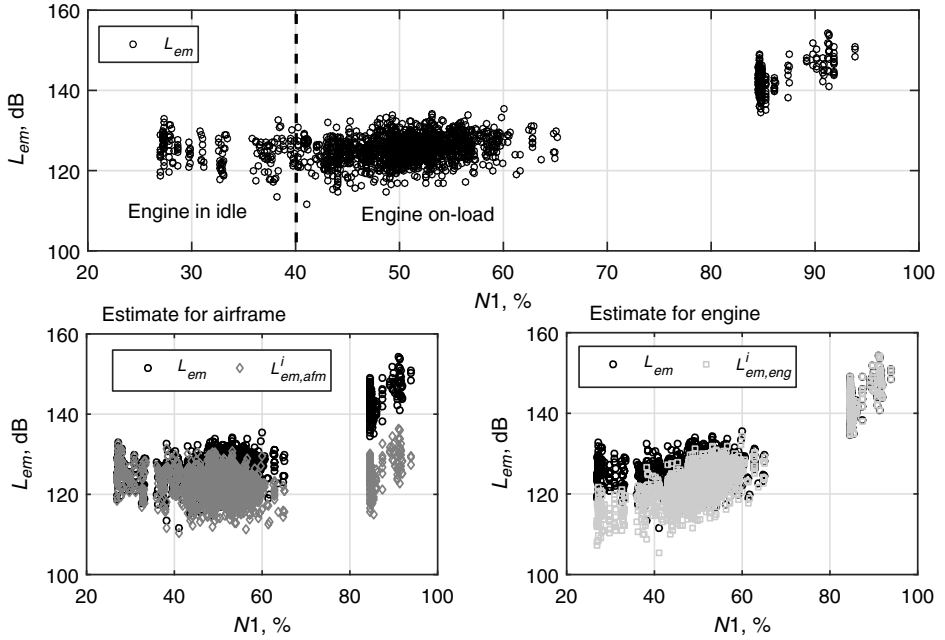

Fig. 9 Data separation example for the A320 at 100 Hz. The backpropagated data (top) are separated to estimates of the sound emission related to airframe (bottom left) and engine noise (bottom right).

In step 5, the final models for airframe and engine noise as defined in Sec. IV are fitted on the separated data sets presented in Fig. 9. Steps 3–5 are repeated once to improve the estimation of the ratio between airframe and engine noise. In the second run, the ratio is based on the models that are fitted on the whole data set in contrast to the ratio based on the initial models. Finally, the energetic sum of the airframe and engine model adds up to the predicted total $\hat{L}_{\mathrm{em}}$. The entire process of data separation and model fitting is performed 24 times to establish models for each 1/3-octave band.

IV. Regression Models

The regression models for airframe and engine noise were developed with the A320 data set, which provides FDR data and a large number of flights, using the modeling approaches presented in Sec. IV.A. The obtained regression models were then tested on the remaining five aircraft types with FDR data to confirm that the models are applicable to different aircraft and engine types. The resulting models are presented as advanced models (Sec. IV.B). In practice, the advanced models are of high level of detail and are therefore well suited to assess or optimize the noise of noise abatement procedures. However, because often no FDR data are available, meaning that the configuration of the aircraft is unknown, also 13 reduced models were established (Sec. IV.C). Those models require less input data and are thus suited for yearly calculations in practice.

A. Modeling Approach and Variables

The choice of variables used to establish the multiple linear regression models is based on the findings of Sec. III.B. These models combine continuous explanatory variables, categorical variables with a certain number of levels, and interactions to predict the dependent variable L_{em}. Interactions are deviations from the additive model describing how the effect of one variable depends on the levels of another variable (e.g., the dependency of the noise emitted by the landing gear on the aircraft Mach number). One important assumption of the linear regression is that the dependent variable is normally distributed. For the logarithmic sound emission level L_{em}, this assumption is fulfilled, whereas it is not for the sound power in watts.

From a statistical point of view, the approach used in this paper equals the forward selection with the scope to only include the relevant variables. To choose the final model, several models with different explanatory variables were compared with respect to the coefficient of determination R^2, the rms error $\hat{\sigma}_E$, and the Akaike information criterion [31]. In doing so, all criteria were compared over 1/3-octave bands to find the most appropriate model. Compliance with the model assumptions, namely, normal distribution and constant variance of the residuals, was visually confirmed by means of residual plots [32].

For the airframe noise model, two transformations were done, applying the base-10 logarithm to the aircraft Mach number (lMa) and to the density ($l\rho$), to fulfill the requirement of a linear relation between the continuous variables and L_{em} (Sec. III.B):

$$lMa = \log_{10}(Ma) \tag{9}$$

$$l\rho = \log_{10}\left(\frac{\rho}{\rho_0}\right) \tag{10}$$

The air density is normalized by the density at mean sea level as defined by the International Standard Atmosphere ($\rho_0 = 1.225\ \mathrm{kg/m^3}$). In practice, Ma is set to 10^{-3} to obtain a real value, and ρ should never be extrapolated to a value near zero. In addition, the landing gear position (LG), the flap handle position (FH), the speedbrakes (SB), and the procedure (Proc) are categorical variables of the airframe noise model. The engine noise model only consists of continuous variables and their interactions, namely Ma, $N1$, $N1^2$, θ, and φ.

B. Advanced Models

The sound emission level of the airframe $\hat{L}_{\mathrm{em,afm}}(f)$ is modeled as the sum of the source terms and the radiation angle terms as summarized in Eq. (11):

$$\hat{L}_{\mathrm{em,afm}}(f) = \underbrace{\hat{L}_{0,\mathrm{afm}}(lMa, l\rho, \mathrm{FH}, \mathrm{LG}, \mathrm{SB}, \mathrm{Proc})}_{\text{source terms}} + \underbrace{\Delta\hat{L}_{\theta,\mathrm{afm}}(\theta)}_{\text{radiation angle terms}} \tag{11}$$

The dependency on the frequency f indicates that all coefficients of the source and radiation angle terms are fitted for all 1/3-octave bands, even if not further denoted for readability. Equation (12) represents the source terms of the airframe model:

$$\hat{L}_{0,\mathrm{afm}} = L_{a0} + a_{a1}\cdot lMa + \mathrm{Proc}\cdot(a_{a2} + a_{a3}\cdot lMa) + b_{a1}\cdot l\rho + \mathrm{LG}\cdot(c_{a1} + c_{a2}\cdot \mathrm{Proc} + c_{a3}\cdot lMa) + \sum_{j=1}^{4}\mathrm{FH}_j\cdot(d_{a1j} + d_{a2j}\cdot \mathrm{LG} + d_{a3j}\cdot \mathrm{Proc}) + \mathrm{SB}\cdot(e_{a1} + e_{a2}\cdot \mathrm{LG} + e_{a3}\cdot lMa) \quad (12)$$

L_{a0} is the intercept, and a_{a1} to e_{a3} are the frequency-dependent coefficients of all model variables. The continuous variables are the logarithmic transformations lMa and $l\rho$, which represent the aeroacoustic sound generation in line with other semi-empirical models [33,34]. In addition, each configuration change of LG, FH, or SB is modeled with additive level changes.

For FH and SB, interactions with the LG are considered to account for the changes in their effect when the sound emission level is raised by the deployed landing gear. Further, interactions between lMa and LG as well as SB are considered to account for the speed-dependent sound generation. For the FH, the interaction with lMa is neglected because each flap handle position is only used for a certain small range of aircraft Mach numbers (Fig. 7), and an interaction with lMa can thus not be determined without high uncertainty.

Nevertheless, the varying combinations of flap handle position and aircraft Mach number range for approach and departure of Fig. 7 need to be considered in the model in one way or another. Further, the different deflection angles of the flap handle position 1 for departures and approaches need to be taken into account. Finally, the observation of the A320 family that 1/3-octave bands with cavity tones can have a strong increase in level with increasing Mach number for approaches but not for departures needs to be considered. It is assumed that the local flowfield is different for approach and departure due to different angle of attack and flap handle positions. To account for these differences, an additional categorical variable, the flight procedure Proc (departure: 1, approach: 0), was introduced.

The directivity of the airframe model [Eq. (13)] is expressed as an axially symmetric radiation along the longitudinal axis of the aircraft because the lateral directivity is mainly assigned to engine noise (discussed later). The polar angle θ is taken into account with a second-order Fourier series to model the longitudinal directivity. The coefficients for the airframe directivity are k_a to n_a. No interactions are included (i.e., the shape of the emission directivity is the same for all flight configurations). This simplification is justified because the data set was already corrected for the flight effect [Eq. (3)]:

$$\Delta\hat{L}_{\theta,\mathrm{afm}} = k_a\cdot\cos\theta + l_a\cdot\cos 2\theta + m_a\cdot\sin\theta + n_a\cdot\sin 2\theta \quad (13)$$

The sound emission level of the engine noise $\hat{L}_{\mathrm{em,eng}}(f)$ is modeled by the sum of source terms and a more detailed approach for the radiation angle terms as summarized in Eq. (14):

$$\hat{L}_{\mathrm{em,eng}}(f) = \underbrace{\hat{L}_{0,\mathrm{eng}}(Ma, N1, N1^2)}_{\text{source terms}} + \underbrace{\Delta\hat{L}_{\theta,\mathrm{eng}}(\theta, N1, N1^2) + \Delta\hat{L}_{\varphi,\mathrm{eng}}(\varphi, N1)}_{\text{radiation angle terms}} \quad (14)$$

Source terms for engine noise [Eq. (15)] include the intercept L_{e0} and three variables with their coefficients a_{e1}, b_{e1}, and b_{e2}. The first source term of engine noise is $N1$. The quadratic approach for $N1$ represents the jet as well as the fan noise as observed in Sec. III.B. In addition, the aircraft Mach number Ma accounts for the source strength variation of the jet mixture with the surrounding flow:

$$\hat{L}_{0,\mathrm{eng}} = L_{e0} + a_{e1}\cdot Ma + b_{e1}\cdot N1 + b_{e2}\cdot N1^2 \quad (15)$$

Because the relation of L_{em} to $N1$ strongly depends on the polar angle θ (Sec. III.B), the Fourier terms of the longitudinal directivity $\Delta\hat{L}_{e\theta,\mathrm{eng}}$ interact with $N1$ as well as $N1^2$ [Eq. (16)]. The corresponding model coefficients are $k_{e,j}$ to $n_{e,j}$ with index j for each interaction. The lateral directivity [Eq. (17)], which represents the installation effect and jet directivity, is included as a half-range Fourier series of second order (i.e., with only sine terms of φ). Similar to the longitudinal directivity, each term has an interaction with $N1$ with coefficients $o_{e,j}$, $p_{e,j}$. Also an interaction with $N1^2$ was tested but not found to significantly improve the results:

$$\Delta\hat{L}_{\theta,\mathrm{eng}} = \left(k_{e,j}\cdot\cos\theta + l_{e,j}\cdot\cos 2\theta + m_{e,j}\cdot\sin\theta + n_{e,j}\cdot\sin 2\theta\right)\cdot(1 + N1 + N1^2) \quad (16)$$

$$\Delta\hat{L}_{\varphi,\mathrm{eng}} = \left(o_{e,j}\cdot\sin\varphi + p_{e,j}\cdot\sin 2\varphi\right)\cdot(1 + N1) \quad (17)$$

With the approach of Eqs. (16) and (17), the shape of the three-dimensional directivity is allowed to change with the engine setting $N1$. Because each 1/3-octave band is fitted separately, also the spectral content of the total directivity varies with the power of the engines.

C. Reduced Models

For the cases when no FDR data are available, the model was reduced by the flight parameters that are unknown. For airframe noise, the configuration parameters are missing and are thus removed from the model approach [Eqs. (18) and (19)]. The effects of the configuration are still implicitly included in the data set. In contrast to the advanced model, the Mach number dependency on L_{em} now accounts for the mean configuration of all measured flights. Thus, the variable Proc is retained in the model due to the same reasons as in Sec. IV.B. The radiation angle terms remain unchanged [Eq. (13)]:

$$\hat{L}_{\mathrm{em,afm}}(f) = \underbrace{\hat{L}_{0,\mathrm{afm}}(lMa, l\rho, \mathrm{Proc})}_{\text{source terms}} + \underbrace{\Delta\hat{L}_{\theta,\mathrm{afm}}(\theta)}_{\text{radiation angle terms}} \quad (18)$$

$$\hat{L}_{0,\mathrm{afm}} = L_{a0} + a_{a1}\cdot lMa + \mathrm{Proc}\cdot(a_{a2} + a_{a3}\cdot lMa) + b_{a1}\cdot l\rho \quad (19)$$

For engine noise, the variable originating from FDR data is $N1$. This variable is crucial because it has the strongest effect on L_{em}. Therefore, in the case of missing FDR data, $N1$ is determined from the spectrogram as shown in [12]. The reduced model for engine noise is thus the same as the advanced model [Eqs. (14–17)].

D. Weighting

During measurements, the polar angle θ changes slowly when the aircraft is far away but quickly while the aircraft overflies the microphone. Consequently, only few data points of the equally spaced acoustical samples are available in the most relevant range of θ and vice versa. When establishing the model coefficients, the weighting reduces the influence of the inhomogeneous distribution of data points over θ. This distribution is inversely proportional to the time derivative $\theta' = \mathrm{d}\theta/\mathrm{d}t$. Analogous to ordinary least squares in linear regression, the models were therefore fitted with the weighted least-squares (WLS) algorithm [32].

Because each flight and receiver combination has a different geometry, θ' was standardized by the maximum value per event and receiver, denoted as $w_{0,i}$ in Eq. (20). The standardization prevents a higher weight of measured levels for an aircraft close to the receiver than far away, where θ' is generally lower. The weights were then normalized by their mean value $\overline{w}_0$ to ensure that the sum of all weights w_i, which are used for the WLS algorithm, matches the number of observations n used in the analysis [Eq. (21)]:

$$w_{0,i} = \theta' / \max(\theta')_{\mathrm{event,receiver}} \quad (20)$$

$$w_i = w_{0,i}/\overline{w}_0 \Rightarrow \sum_{1}^{n} w_i = n \quad (21)$$

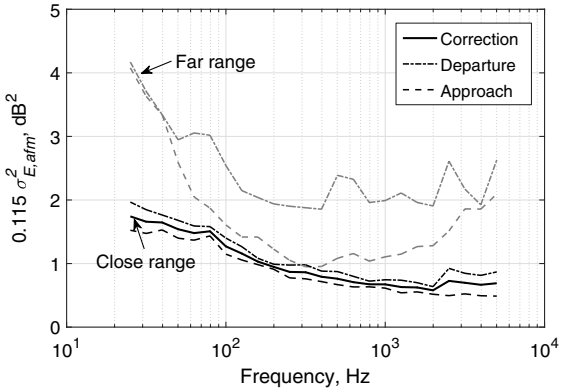

Fig. 10 Correction factor for energy mean vs frequency for the A320.

Because the regression coefficients of the advanced and reduced models are estimated with the WLS algorithm, also the coefficient of determination R^2 and the error mean square $\hat{\sigma}_E^2$ are weighted using Eqs. (22) and (23); compare [32]. $L_{\mathrm{em},i}$ represents the backpropagated data, and $\hat{L}_{\mathrm{em},i}$ represents the corresponding predicted values [Eq. (26)] for n observations and m explanatory variables:

$$R^2 = 1 - \frac{\sum_{i=1}^{n} w_i (L_{\mathrm{em},i} - \hat{L}_{\mathrm{em},i})^2}{\sum_{i=1}^{n} w_i (L_{\mathrm{em},i} - \overline{L}_{\mathrm{em},i})^2} \tag{22}$$

$$\hat{\sigma}_E^2 = \frac{1}{n-(m+1)} \sum_{i=1}^{n} w_i (L_{\mathrm{em},i} - \hat{L}_{\mathrm{em},i})^2 \tag{23}$$

E. Energy Correction

As a consequence of the least-squares estimation, the model predicts the arithmetic mean of the sound emission level L_{em} in decibels. A correction is needed to predict the energy mean $L_{\overline{\mathrm{em}}}$, which is equal to the arithmetic mean of the sound power in watts. Because L_{em} is normally distributed (Sec. IV.A), the energy correction can be analytically determined by $0.115 \cdot \sigma^2$ [30,35].

The variance σ^2 can be represented by the error variance estimate $\hat{\sigma}_E^2(f)$ of each regression model. Figure 10 shows that the error variance is considerably larger for microphones in the far range than in the close range, which is mainly caused by atmospheric turbulence and uncertainty in backpropagation. In general, microphones for departures in the far range are more distant from the source, which further supports the interpretation that the variance is distance-dependent. The energy correction should only include the variance of the source and uncertainty of the measurements, which are not distance-dependent. Therefore, the correction was applied for the error variance of the data in the close range, which is assumed to be dominated by the variance of the source. The total error variance of approach and departure in the close range (CR) is applied for each model as defined by Eqs. (24) and (25):

$$\hat{L}_{\overline{\mathrm{em}},\mathrm{afm}}(f) = \hat{L}_{\mathrm{em},\mathrm{afm}}(f) + 0.115 \cdot \hat{\sigma}^2_{E,\mathrm{afm,CR}}(f) \tag{24}$$

$$\hat{L}_{\overline{\mathrm{em}},\mathrm{eng}}(f) = \hat{L}_{\mathrm{em},\mathrm{eng}}(f) + 0.115 \cdot \hat{\sigma}^2_{E,\mathrm{eng,CR}}(f) \tag{25}$$

The energetic sum $\oplus$ of the fitted models for airframe [Eq. (24)] and engine noise [Eq. (25)] results in the total predicted emission spectra of the modeled aircraft type (step 6 in Fig. 8):

$$\hat{L}_{\overline{\mathrm{em}},\mathrm{total}}(f) = \hat{L}_{\overline{\mathrm{em}},\mathrm{afm}}(f) \oplus \hat{L}_{\overline{\mathrm{em}},\mathrm{eng}}(f) \tag{26}$$

V. Results

In this section, we introduce the established aircraft noise emission models, which are based on either individual aircraft types or groupings of similar aircraft types with the same engine type. Their model performance is shown by the coefficient of determination and rms error. Finally, several predictions of typical flight configurations are compared to measured data to validate the model.

A. Established Aircraft Types

In total, regression models for 19 aircraft types were established on the basis of the input data presented in Sec. II. Table A1 gives an overview on the grouped aircraft and engine types, the data origin, and the number of flights that the models are based on. For instance, the Airbus A320-200 equipped with CFM56-5B is based on FDR data and 673 flights in total. Another example is the Embraer E170, based on $N1$ determination instead of FDR data with 89 flights in total. Both types are used frequently in the following account for illustrative purposes and to show the feasibility of the advanced and reduced model.

Some aircraft types of the same aircraft family were grouped when the number of measured flights was low. As a rule, only types with the same engine are grouped because the engines are the main sound source that can lead to considerably different sound emission. For instance, all subtypes of the B737 with the classic engine option CFM56-3 are grouped, whereas all types of the new generation equipped with modern CFM56-7B are grouped separately. Grouping of an aircraft family is reasonable and improves the model because a wider range of flight parameters is covered due to different takeoff weights and procedures and thus different $N1$ for departures. This improves the parameter range that the model is build on.

B. Model Performance

The model performance is assessed with the coefficient of determination R^2 and the rms error $\hat{\sigma}_E$. R^2 is a dimensionless measure for the variance explained by the selected parameters in each 1/3-octave band. $\hat{\sigma}_E$ provides the same unit (decibels) as the sound emission level and assesses the unexplained variation in each 1/3-octave band. R^2_{total} represents the model performance of the sum of the predicted values [Eq. (26)] to reproduce the original set of backpropagated data L_{em}. R^2_{afm} and R^2_{eng} are helpful for qualitative considerations. They have to be regarded with care because they are calculated with respect to the separated data set, which was separated by those models.

Figure 11 depicts the coefficients of determination R^2 for the 24 models (one per 1/3-octave band). Overall, R^2_{total} indicates good explanatory power of the regression models with values between 0.7 and 0.8 for the A320 and also for the E170. The engine model shows R^2_{eng} values slightly larger than 0.8 for most 1/3-octave bands. In contrast, the airframe model of the A320 has R^2_{afm} values between 0.2 and 0.6, with much more variation between the different 1/3-octave bands. For the E170, R^2_{afm} is generally higher and varies between 0.4 and 0.7.

A specific aspect of R^2 is related to the frequency range in which the sound sources radiate. For instance, R^2_{eng} of the A320 in Fig. 11a is high, between 50 and 400 Hz, where the jet noise is dominant; this is in line with [36]. Similarly, R^2_{eng} is high at 2–3 kHz, the 1/3-octave bands that contain the blade-passing frequency (BPF) of the A320 at departure. Airframe sound sources can be identified in the same manner. In accordance with measurements on an A320 full-scale wing [34], the slats (included by the variable FH) radiate considerable sound power between 100 and 300 Hz. Furthermore, a prominent cavity tone in the wing radiates at 500 and 630 Hz. Finally, excess noise of the flap-side edge is prominent between 1 and 1.6 kHz. Exactly in those frequency ranges, R^2_{afm} shows local maxima. In contrast, no explicit sound sources for 50 to 100 Hz and above 1.6 kHz exist, and consequently, R^2_{afm} is low. For the E170, there are no measurements that are similar to the known measurements for the A320, but Fig. 11b shows a tone at 100 Hz that also increases the R^2_{afm}. In general, the high values of R^2_{afm} of the E170 indicate that airframe sound sources contribute in almost all 1/3-octave bands.

Figure 12 shows that the total $\hat{\sigma}_E$ for the A320 and E170 lies between 4.5 dB for low frequencies and around 3 dB for mid- and high frequencies. Because the variance of the input data was found to be large (Sec. III.B), $\hat{\sigma}_E$ is also relatively large. The unexplained variations are thus partly explained by the uncertainties of the

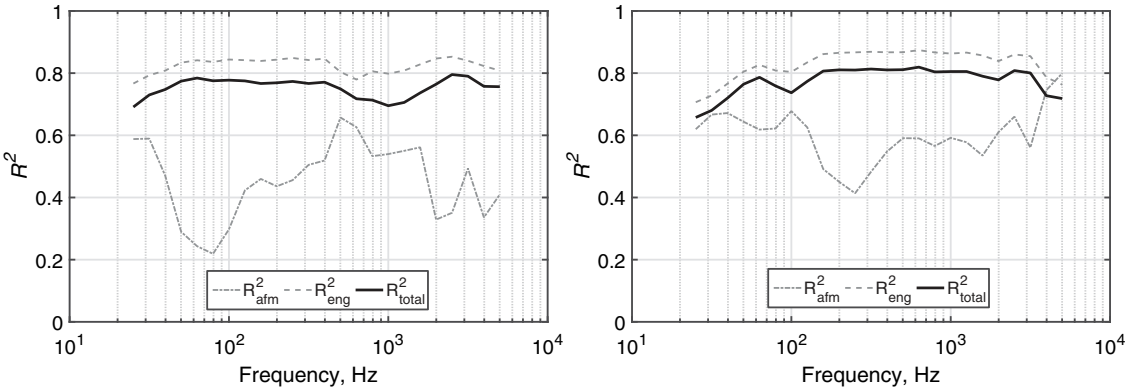

a) A320 based on FDR data **b) E170 without FDR data**

Fig. 11 Coefficient of determination vs frequency for airframe, engine, and total model.

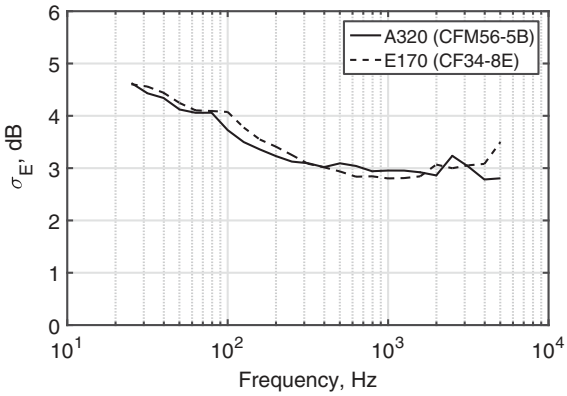

Fig. 12 RMS error for the A320 and E170.

measurement and the backpropagation, variation of the source, and atmospheric turbulence. This is supported by the fact that both aircraft types with the advanced as well as reduce regression model show similar values of $\hat{\sigma}_E$.

C. Model Comparison

In this section, example model predictions of spectra and directivity patterns are shown for various flight configurations and compared to measurements. For comparison of model predictions with the measured data, the data set is filtered as follows. Flight parameters for the flight phase and a radiation angle of interest are chosen to predict the sound emission level. Then, the same parameters with a certain interval around each parameter are used to create a subset from the complete data set ($\varphi = 60\pm5$ deg, $N1 = 93\pm2\%$, etc.). Finally, the arithmetic mean L_{em} is calculated and compared with the arithmetic mean of the predicted values $\hat{L}_{\text{em}}$ (see Sec. IV.E). Hence, the large variations of the measured data in Sec. III.B are averaged for the comparison. This comparison allows assessing whether the model approach is appropriate, even if it is not an independent comparison because the model was fitted on the same data set.

In Fig. 13, spectral directivity patterns for a departure with a high-power setting of $N1 = 93\%$ are shown. The longitudinal directivity in Fig. 13a is presented for an observer on the side at $\varphi = 60$ deg. All $1/3$-octave bands show a good agreement between predicted and measured data. Low frequencies, such as 125 and 250 Hz, show the typical jet characteristic [37] that is pronounced to the rear ($\theta \approx 120$–150 deg). For high frequencies, such as 2 kHz, the directivity pattern has local maxima to the front and rear due to the fan. Hence, the Fourier series and the interactions with $N1$ and $N1^2$ allow the model to accurately represent the longitudinal directivity.

In the same way, the lateral directivity, shown from the rear at $\theta = 130$ deg in Fig. 13b, agrees well with the measurements. Overall, the lateral radiation is less pronounced and less variable over the $1/3$-octave bands. Thus, the half-range Fourier series with interaction to $N1$ is a valid approach. Longitudinal and lateral directivity also agree very for the overall L_{em} as presented in [38], which further supports the chosen model approach for the directivity.

In Fig. 14, spectra for typical flight configurations of takeoff and final approach are depicted below the aircraft (Fig. 14a) and to the rear (Fig. 14b). As expected, the dominant sound source at takeoff is the engine. The airframe model is not shown for this case to avoid an overlap with the spectra of the final approach. The low-frequency broadband noise of the jet in the rear as well as the BPF at 2.5 kHz are represented well. In contrast to departure, the airframe model is relevant for the final approach. In Fig. 14a, the midfrequencies are still dominated by engine noise, probably turbomachinery noise, whereas at the rear in Fig. 14b, airframe noise dominates the midfrequencies. Interestingly, although jet noise is very low for $N1 = 55\%$, the broadband noise of the fan can still be found around 4 kHz in the engine spectra for final approach.

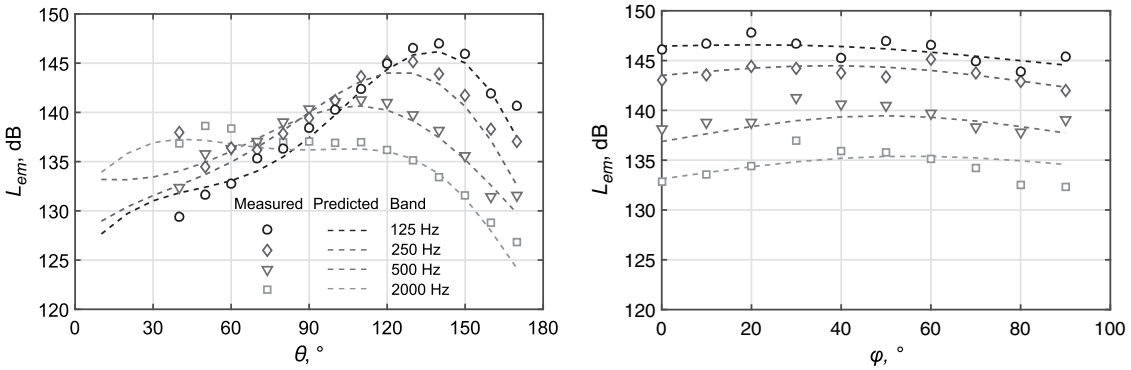

a) Longitudinal directivity ($\varphi = 60°, N1 = 93\%$) **b) Lateral directivity ($\theta = 130°, N1 = 93\%$)**

Fig. 13 Spectral directivity patterns of the A320 for departure at high-power setting.

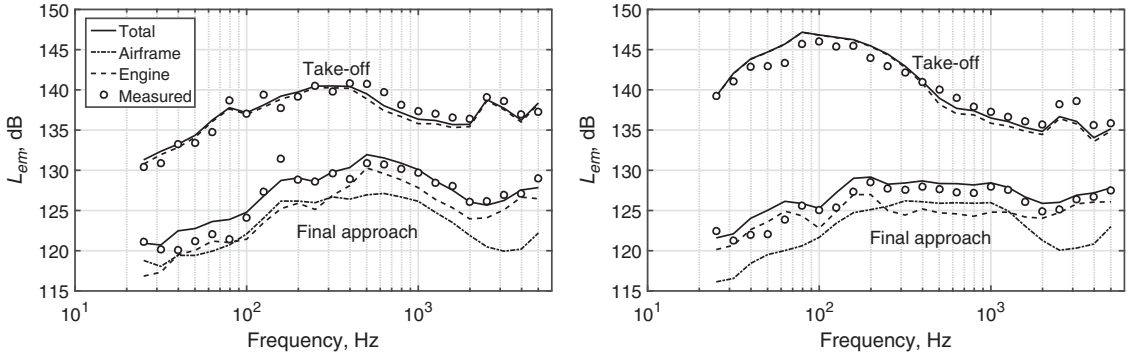

a) Spectra below the aircraft at $\theta = 90°$ b) Spectra in the rear at $\theta = 130°$

Fig. 14 Spectra for final approach ($N1 = 55\%$, $Ma = 0.23$) and takeoff at high-power setting ($N1 = 93\%$, $Ma = 0.24$) for the A320.

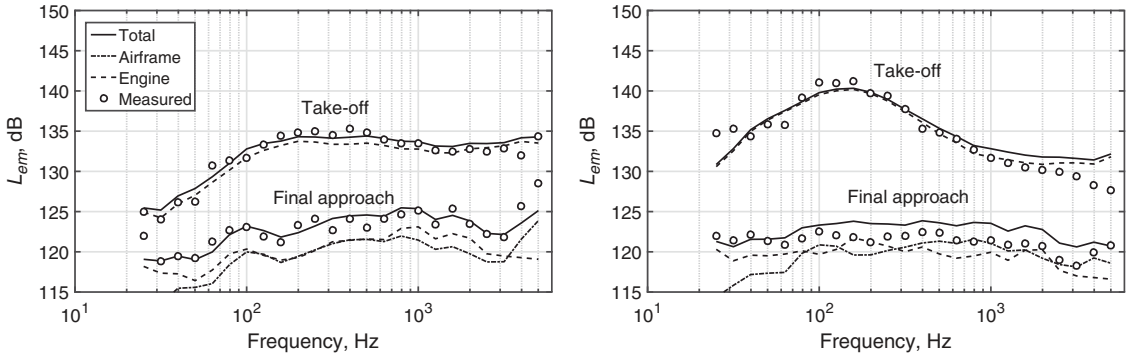

a) Spectra below the aircraft at $\theta = 90°$ b) Spectra in the rear at $\theta = 130°$

Fig. 15 Spectra for final approach ($N1 = 50\%$, $Ma = 0.2$) and takeoff at high-power setting ($N1 = 86\%$, $Ma = 0.24$) for the E170.

The corresponding spectra of the E170 in Fig. 15 depict similar model performance. The total spectra are in good agreement with the measurements, and departures are dominated by engine noise. At typical final approach settings, engine and airframe noise contribute equally over all frequencies in contrast to the source-dependent contributions of the A320. For departure, the BPF at 3 kHz is not observed in either Fig. 15a or Fig. 15b, which is in line with the measurements. For the final approach, the BPF can be found in Fig. 15a at 1.7 kHz in the prediction as well as in the measurement.

D. Example Application to Approach Procedures

In the following example, the advanced regression model for A320 (CFM56-5B) is applied within a simulation program that accounts for the sound propagation using sonX (Sec. II.B), the flight effect, and the Doppler shift. Although all other results in this paper were shown as emissions, a noise map was calculated here on a receiver grid with 150 m spacing in an area of 60×32 km. To highlight the observable effects of the noise emission model, an artificial airport was modeled with a flat grassland terrain and a homogenous atmosphere ($T = 14°\text{C}$, $p = 1000$ hPa, $rH = 60\%$).

In the example in Fig. 16, two approach procedures are compared: a low-drag, low-power (LDLP) approach versus a continuous-descent approach (CDA). The noise map shows noise contours as well as the differences $\Delta L_{\text{AS,max}}$ between the CDA and the LDLP approach, where positive differences mean that the CDA has larger maximum levels than the LDLP approach. This is the case between 56 to 40 km and on the glide path between 21 and 10 km. To highlight the differences due to the sound emission rather than to different horizontal tracks, both approach procedures were simulated along the same flight path. The differences $\Delta L_{\text{AS,max}}$ under the flight path and the flight parameters such as altitude, aircraft Mach number, $N1$, and configuration are depicted in Fig. 17. Additionally, in Figs. 16 and 17, the same distance markers are depicted to connect the resulting $\Delta L_{\text{AS,max}}$ noise map with the flight parameters. The markers refer to the flight-path distance, where 0 m is at the end of the runway.

The calculation shows that the flight parameters strongly affect the results and that they need to be considered to compare different noise abatement procedures. For instance, far away from the runway (greater than 56 km), the CDA is quieter than the LDLP because the engines are running in idle. Between 56 and 40 km, CDA is louder due to the lower altitude and the higher sound emission by the airframe (Mach number) and engines ($N1$). In the subsequent segment (40–26 km), the CDA is again quieter than LDLP because of the higher altitude, but also the high-lift devices are deployed later. Between 26 and 21 km, the differences tend around zero because the airframe noise (larger Mach number) of the CDA is compensated by the engine noise (larger $N1$) of the LDLP approach. Although the altitude after 21 km is the same for both approaches on the glide path, the higher aircraft Mach number of the CDA leads again to positive differences. In the final segment, no differences can be found because all flight parameters are the same. Note that it was not the scope of this calculation to systematically evaluate CDA and LDLP, because the results only reflect the specific flight parameters used for this example, but to illustrate the application of the noise emission model.

VI. Discussion

In this paper, a new aircraft noise emission model is presented that overcomes the limitations in prediction of today's aircraft noise models with a moderate number of necessary input parameters. As a major advantage to models such as to Doc. 9911 [2], Doc. 29 [30], or FLULA2 [5], airframe noise (predicted by the aircraft Mach number and configuration) is separately modeled from the engine noise. At the same time, only two flight parameters ($N1$, Mach number) are needed for engine noise; thus, no detailed knowledge of the engine performance such as mass flow or jet speed is required as for the high-end models ANOPP [7] or PANAM [9]. Jet and fan noise of the engines are considered by $N1$ as the main parameter, which is in line with the findings of Simons et al. [39], who suggested to incorporate the engine setting via $N1$ into new acoustical models. As a further advantage, $N1$ can be determined acoustically [12] to develop the models.

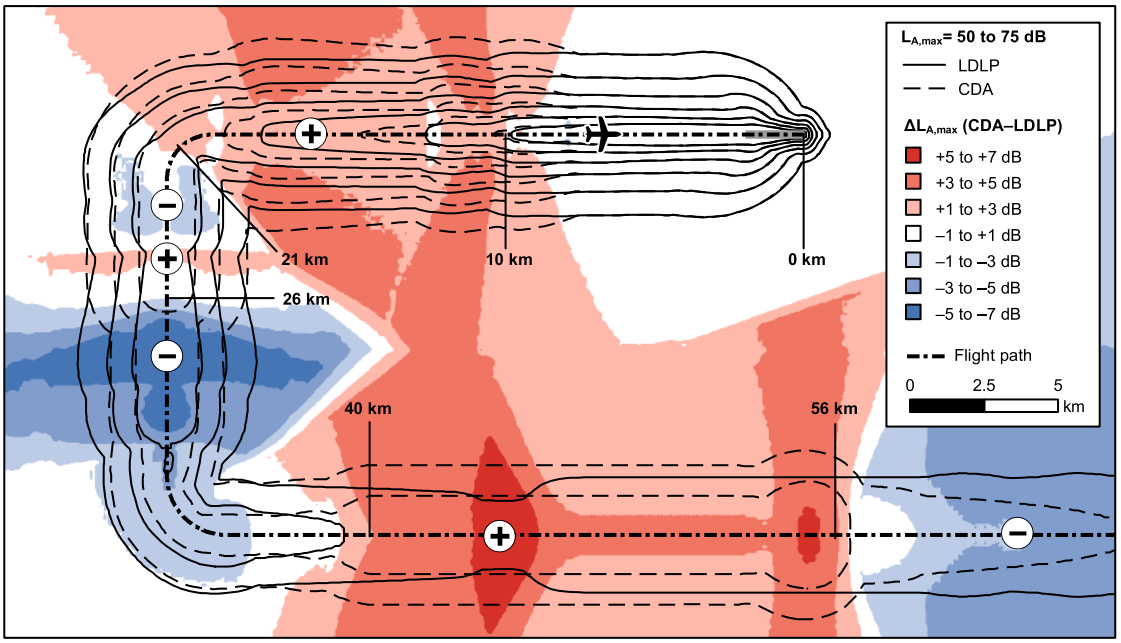

Fig. 16 Example comparison of a CDA and LDLP approach procedure for the A320 (CFM56-5B). The noise map depicts the differences $\Delta L_{A,\max}$ between CDA and LDLP approach.

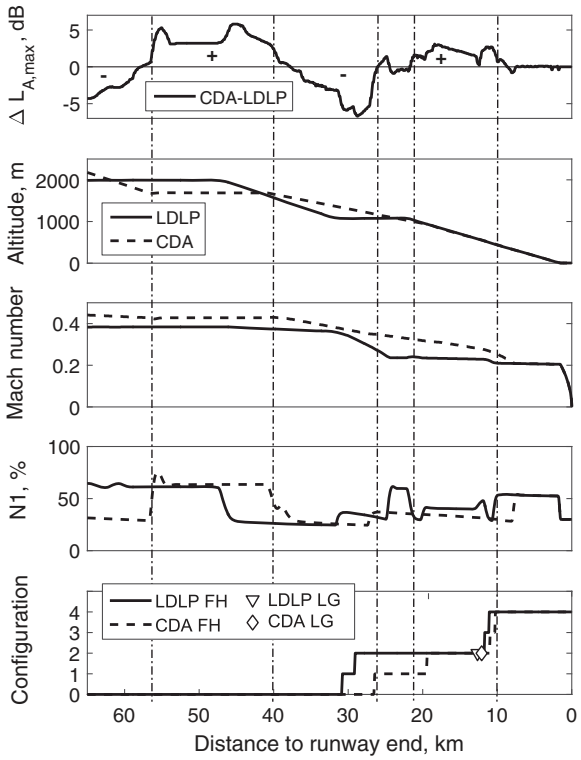

Fig. 17 $\Delta L_{A,\max}$ between CDA and LDLP approach versus flight track distance and corresponding flight parameters of the A320 (CFM56-5B). The vertical distance markers correspond to those of Fig. 16.

The regression models were fitted in an iterative process, where the total sound emission levels were separated to airframe and engine noise. On this basis, new combinations of modeled (existing) airframes and engines, for which input data are missing or which are not yet flying in such combination, can be established. A further refinement to detailed modeling of single sound sources, as done in [34], is still challenging, especially with the scope to cover a wide range of aircraft types with different dimensions [40]. However, this was beyond the scope of the study, where the objective was to develop a general aircraft noise emission model to reliably predict the total sound emission and the contributions from airframe and engine sources separately.

The results demonstrated that this objective is achieved because the chosen model variables allow to adequately reproduce the directivity and spectra for typical flight configurations. These results are valid for the known data range; however, extrapolation of the model parameters is uncertain and not validated. Interestingly, the A320 with FDR data and a large number of flights as well as the E170 without FDR data and only 89 flights showed similarly good results. This was the case for all aircraft types in Table A1. Thus, the performance of the advanced and reduced models is comparable, meaning that reliably models may be established from input data of different degrees of detail.

Where available, it is recommended to use the advanced model for studies on single-flight procedures, for instance by using data from flight mechanical calculations or full-flight simulators, which usually provide the required parameters of the model. Nevertheless, the reduced model is similarly applicable, although the effect of changing aeroplane configuration cannot be accounted for. However, at least for airport scenarios and yearly calculations, the reduced model is likely to improve the accuracy of today's noise maps compared to best practice programs due to the following reasons. First, the aircraft Mach number is accounted for, which correlates with the effects of the configuration of the airframe and thus is a proxy for the latter. Second, the model is based on measurements up to 20 km from the airport and is thus reliable to a large range of flight parameters.

Current research strongly focuses on the optimization of new aircraft concepts, investigating blended wing-body aircraft [41] and hybrid wing-body aircraft [42] using ANOPP [7] and ANOPP2 [43], or economic and environmental efficiency of new aircraft concepts [44] using PANAM [9]. Predicting new aircraft concepts justifies the high level of detail of the applied semi-empirical models and the number of input parameters. In contrast, the presented aircraft noise emission model is limited to existing aircraft types because it is based on empirical data.

The applicability of the aircraft noise emission model on a specific airport is currently limited by the available aircraft types, as the effort is large to establish additional aircraft types. The prerequisites to establish the model for new aircraft types are 1) measurements at different locations close to and far from an airport, 2) backpropagation

to the source, and 3) spectral analysis to determine $N1$ or processing FDR data. It is thus costly to establish an additional aircraft type but feasible as already demonstrated for 19 aircraft types. Furthermore, the separation of airframe and engine noise is limited to the assumption that airframe noise dominates if the engines are running in idle. The validity of this assumption and the resulting separation still needs to be proved, for instance with array measurement such as in [45,46].

In practice, new procedures such as the CDA can be compared to existing procedures and optimized acoustically by means of the presented aircraft noise emission model. Example results showed that the effects of flight parameters on the sound emission at approach are much more important than mere changes in altitude. This is a major advantage to best practice programs (Doc. 9911, FLULA2), which cannot account for those effects [6]. The model could thus be used to extend current studies on trajectory optimization with noise as a cost function [47,48].

VII. Conclusions

In this paper, an aircraft noise emission model was established for a wide range of relevant aircraft and engine types, which showed the general applicability of the modeling approach. The model describes the sound emission in great detail as spectral three-dimensional directivity patterns in function of flight parameters, separately for airframe and engine noise. The model fills the gap between existing best practice programs and high-end models.

Two regression models with different levels of detail and different applicability were derived. The advanced model is suitable to optimize and assess the noise of new noise abatement procedure in great detail. However, its application is limited by the availability of flight data records to establish the model. In case such data are missing, a reduced model can be established, which will still improve the accuracy of today's noise maps because it includes important flight parameters and is based on extensive measurements covering a wide range of flight configurations.

Ongoing research focuses on the validation of the model with independent measurements. Besides, the methodology to separate airframe and engine noise should be validated, for instance with sophisticated data from array measurements. Furthermore, it would be desirable to use the presented modeling approach to develop aircraft noise emission models for helicopters, propeller-driven airplanes, or military jets. If and how the approach can be adapted to that purpose needs to be tested.

Appendix

Table A1 Established regression models with input data basis and number of flights

Aircraft type	Engine type	Input	Departure	Approach	Total
Airbus A319-100	CFM56-5B	FDR	120	41	161
Airbus A320-200	CFM56-5B	FDR	424	249	673
Airbus A321-200	CFM56-5B	FDR	300	126	426
Airbus A320 family	CFM56-5A	N1	57	15	72
Airbus A320 family	V2500	N1	198	33	231
Airbus A330-300	TRENT7	FDR	249	136	385
Airbus A340-300	CFM56-5C	FDR	166	120	286
Airbus A380-800	GP7270	N1	26	2	28
Airbus A380-800	TRENT9	N1	38	20	58
BAe Avro RJ-100	LF507	FDR	324	202	526
Boeing B737 Classic	CFM56-3	N1	84	39	123
Boeing B737 NG	CFM56-7B	N1	297	37	334
Boeing 767-300	PW4060	N1	9	34	43
Boeing 767 family	CF6-80C2	N1	19	57	76
Bombardier CRJ-900	CF34-80C2	N1	71	22	93
Dassault Falcon 7X	PW307	N1	17	10	27
Embraer ERJ 170	CF34-8E	N1	62	27	89
Embraer ERJ 190	CF34-10E	N1	243	49	292
Fokker 100	TAY650-15	N1	234	61	295

Acknowledgments

This research was funded by the Federal Office of Civil Aviation, Empa, the Swiss Civil Air Traffic Control (skyguide), the Office of Transport of the canton of Zurich, Zurich Airport, and Geneva International Airport. The authors address special thanks to Swiss International Air Lines and to Zurich Airport for their great support of the project by providing data and participating in the measurements. We thank Markus Studer for his excellent technical assistance, Scott Whiteford for the language editing, and all our colleagues and partners involved in the project sonAIR.

References

[1] "Guidance on the Balanced Approach to Aircraft Noise Management," International Civil Aviation Organization, Doc. 9829 AN/451, Montreal, 2008.

[2] "Recommended Method for Computing Noise Contours Around Airports," International Civil Aviation Organization, Doc. 9911, Montreal, 2008.

[3] "Anleitung zur Berechnung von Lärmschutzbereichen," Bundesrat Rept. 588/08, Bundesrat, Germany, 2008.

[4] Isermann, U., and Vogelsang, B., "AzB and ECAC Doc. 29—Two Best-Practice European Aircraft Noise Prediction Models," *Noise Control Engineering Journal*, Vol. 58, No. 4, 2010, pp. 455–461. doi:10.3397/1.3455442

[5] Krebs, W., Bütikofer, R., Plüss, S., and Thomann, G., "Sound Source Data for Aircraft Noise Simulation," *Acta Acustica United with Acustica* Vol. 90, No. 1, 2004, pp. 91–100.

[6] Schäffer, B., Zellmann, C., Krebs, W., Plüss, S., Eggenschwiler, K., Bütikofer, R., and Wunderli, J. M., "Sound Source Data for Aircraft Noise Calculations State of the Art and Future Challenges," *Proceedings of Euronoise 2012, 9th European Conference on Noise Control*, European Acoustic Assoc., Madrid, 2012, pp. 589–594.

[7] Kontos, K. B., Janardan, B. A., and Gliebe, P. R., "Improved NASA-ANOPP Noise Prediction Computer Code for Advanced Subsonic Propulsion Systems. Volume 1: ANOPP Evaluation and Fan Noise Model," NASA CR-195480, 1996.

[8] Isermann, U., Matschat, K., and Mueller, E. A., "Prediction of Aircraft Noise Around Airports by a Simulation Procedure," *Proceedings of the International Conference on Noise Control Engineering, Progress in Noise Control: INTER-NOISE 1986*, Vol. 1, 1986, pp. 717–722.

[9] Bertsch, L., Dobrzynski, W., and Guérin, S., "Tool Development for Low-Noise Aircraft Design," *Journal of Aircraft*, Vol. 47, No. 2, 2010, pp. 694–699. doi:10.2514/1.43188

[10] Bertsch, L., and Isermann, U., "Noise Prediction Toolbox Used by the DLR Aircraft Noise Working Group," *Proceedings of the 42nd International Congress and Exposition on Noise Control Engineering 2013, INTER-NOISE 2013: Noise Control for Quality of Life*, Vol. 247, No. 8, Inst. of Noise Control Engineering, Washington, D.C., 2013, pp. 805–813.

[11] Zellmann, C., Wunderli, J. M., and Schäffer, B., "SonAIR–Data Acquisition for a Next Generation Aircraft Noise Simulation Model," *Proceedings of INTER-NOISE 2013—42nd International Congress and Exposition on Noise Control Engineering: Noise Control for Quality of Life*, Vol. 247, No. 6, Inst. of Noise Control Engineering, Washington, D.C., 2013, pp. 2044–2052.

[12] Schlüter, S., and Becker, S., "Determination of Aircraft Engine Speed Based on Acoustic Measurements," *Proceedings of INTER-NOISE 2016—45th International Congress on Noise Control Engineering: Towards a Quieter Future*, Vol. 253, No. 4, Inst. of Noise Control Engineering, Washington, D.C., 2016, pp. 4366–4373.

[13] Heutschi, K., "SonRoad: New Swiss Road Traffic Noise Model," *Acta Acustica United with Acustica*, Vol. 90, No. 3, 2004, pp. 548–554.

[14] Thron, T., and Hecht, M., "The sonRAIL Emission Model for Railway Noise in Switzerland," *Acta Acustica United with Acustica*, Vol. 96, No. 5, 2010, pp. 873–883. doi:10.3813/AAA.918346

[15] Wunderli, J. M., Pieren, R., and Heutschi, K., "The Swiss Shooting Sound Calculation Model sonARMS," *Noise Control Engineering Journal*, Vol. 60, No. 3, 2012, pp. 224–235.

[16] Wunderli, J. M., "sonRAIL—From the Scientific Model to an Application in Practice," *Proceedings of Euronoise 2012, 9th European Conference on Noise Control*, European Acoustic Assoc., Madrid, 2012, pp. 475–480.

[17] Zellmann, C., and Wunderli, J. M., "Influence of the Atmospheric Stratification on the Sound Propagation of Single Flights," *Proceedings*

of INTER-NOISE 2014—43rd International Congress on Noise Control Engineering: Improving the World Through Noise Control, Vol. 249, No. 4, Inst. of Noise Control Engineering, Washington, D.C., 2014, pp. 3770–3779.

[18] Stone, J. R., "Flight Effects on Exhaust Noise for Turbojet and Turbofan Engines—Comparison of Experimental Data with Prediction," NASA TM-X-73552, 1976.

[19] Merriman, J., Good, R., Low, J., Yee, P., and Blankenship, G. L., "Forward Motion and Installation Effects on Engine Noise," *3rd Aeroacoustics Conference*, AIAA Paper 1976-0584, 1976.

[20] Filzmoser, P., Garrett, R. G., and Reimann, C., "Multivariate Outlier Detection in Exploration Geochemistry," *Computers and Geosciences*, Vol. 31, No. 5, 2005, pp. 579–587. doi:10.1016/j.cageo.2004.11.013

[21] Lighthill, M. J., "On Sound Generated Aerodynamically. 1. General Theory," *Proceedings of the Royal Society of London A: Mathematical, Physical and Engineering Sciences*, Vol. 211, No. 1107, 1952, pp. 564–587. doi:10.1098/rspa.1952.0060

[22] Stone, J. R., "Interim Prediction Method for Jet Noise," NASA TM-X-71618, 1974.

[23] Guérin, S., and Michel, U., "Aero-Engine Noise Investigated from Flight Tests," *12th AIAA/CEAS Aeroacoustics Conference*, AIAA Paper 2006-2463, May 2006.

[24] Heidmann, M. F., "Interim Prediction Method for Fan and Compressor Source Noise," NASA TM X-71763, 1979.

[25] Ribner, H. S., "The Generation of Sound by Turbulent Jets," *Advances in Applied Mechanics*, Vol. 8, No. C, 1964, pp. 103–182. doi:10.1016/S0065-2156(08)70354-5

[26] Plovsing, B., and Svane, C., "Aircraft Noise Exposure Prediction Model: Guidelines for the Methodology of a Danish Computer Program," Danish Acoustical Inst., Rept. 101, Lyngby, 1983.

[27] Gaumain, C., "Prediction of Noise in the Vicinity of an Airport: A Simulation Method Based on Frequency Dependent Directivity Patterns," KTH Royal Inst. of Technology, Rept. TRITA-FKT 1998:311, Stockholm, 1998.

[28] Neter, J., Nachtsheim, C. J., and Kutner, M. H., "Building the Regression Model 2: Diagnostics," *Applied Linear Regression Models*, 4th ed., McGraw–Hill, Maidenhead, England, U.K., 2004, pp. 384–420.

[29] Krebs, W., Bütikofer, R., Plüss, S., and Thomann, G., "Spectral Three-Dimensional Sound Directivity Models for Fixed Wing Aircraft," *Acta Acustica United with Acustica*, Vol. 92, No. 2, 2006, pp. 269–277.

[30] "Report on Standard Method of Computing Noise Contours Around Civil Airports, Volume 2: Technical Guide," 4th ed., European Civil Aviation Conference Doc. 29, Neuilly-sur-Seine, France, Dec. 2016.

[31] Akaike, H., "Information Theory and an Extension of the Maximum Likelihood Principle," *Selected Papers of Hirotugu Akaike*, Springer, New York, 1998, pp. 199–213.

[32] Neter, J., Nachtsheim, C. J., and Kutner, M. H., "Building the Regression Model 3: Remedial Measures," *Applied Linear Regression Models*, 4th ed., McGraw–Hill, Maidenhead, England, U.K., 2004, pp. 421–480.

[33] Bertsch, L., Guérin, S., Looye, G., and Pott-Pollenske, M., "The Parametric Aircraft Noise Analysis Module–Status Overview and Recent Applications," *17th AIAA/CEAS Aeroacoustics Conference 2011*, AIAA Paper 2011-2855, June 2011.

[34] Pott-Pollenske, M., Dobrzynski, W., Buchholz, H., Guérin, S., Saueressig, G., and Finke, U., "Airframe Noise Characteristics from Flyover Measurements and Predictions," *12th AIAA/CEAS Aeroacoustics Conference*, AIAA Paper 2006-2567, May 2006.

[35] Barry, T. M., and Reagan, J. A., "FHWA Highway Traffic Noise Prediction Model," Federal Highway Administration Rept. FHWA-RD-77-108, Washington, D.C., Dec. 1987.

[36] Blankenship, G. L., Low, J. K. C., Watkins, J. A., and Merriman, J. E., "Effect of Forward Motion on Engine Noise," NASA CR-134954, 1977.

[37] Michel, U., and Michalke, A., "Prediction of Flyover Jet Noise Spectra from Static Tests," NASA TM-83219, 1981.

[38] Zellmann, C., Wunderli, J. M., and Paschereit, C. O., "The sonAIR Sound Model: Spectral Three-Dimensional Directivity Patterns in Dependency of the Flight Condition," *Proceedings of INTER-NOISE 2016—45th International Congress on Noise Control Engineering: Towards a Quieter Future*, Vol. 253, No. 4, Inst. of Noise Control Engineering, Washington, D.C., 2016, pp. 4348–4356.

[39] Simons, D. G., Snellen, M., Midden, B. V., Arntzen, M., and Bergmans, D. H. T., "Assessment of Noise Level Variations of Aircraft Flyovers Using Acoustic Arrays," *Journal of Aircraft*, Vol. 52, No. 5, 2015, pp. 1625–1633. doi:10.2514/1.C033020

[40] Dobrzynski, W., Ewert, R., Pott-Pollenske, M., Herr, M., and Delfs, J., "Research at DLR Towards Airframe Noise Prediction and Reduction," *Aerospace Science and Technology*, Vol. 12, No. 1, 2008, pp. 80–90. doi:10.1016/j.ast.2007.10.014

[41] Guo, Y., Burley, C. L., and Thomas, R. H., "On Noise Assessment for Blended Wing Body Aircraft," *52nd Aerospace Sciences Meeting*, AIAA Paper 2014-0365, 2014.

[42] Thomas, R. H., Burley, C. L., and Olson, E., "Hybrid Wing Body Aircraft System Noise Assessment with Propulsion Airframe Aeroacoustic Experiments," *International Journal of Aeroacoustics* Vol. 11, Nos. 3–4, 2012, pp. 369–409. doi:10.1260/1475-472X.11.3-4.369

[43] Lopes, L. V., and Burley, C. L., "Design of the Next Generation Aircraft Noise Prediction Program: ANOPP2," *17th AIAA/CEAS Aeroacoustics Conference*, AIAA Paper 2011-2854, June 2011.

[44] Bertsch, L., Heinze, W., and Lummer, M., "Application of an Aircraft Design-to-Noise Simulation Process," *14th AIAA Aviation Technology, Integration, and Operations Conference*, AIAA Paper 2014-2169, 2014.

[45] Guérin, S., Michel, U., Siller, H., Finke, U., and Saueressig, G., "Airbus A319 Database from Dedicated Flyover Measurements to Investigate Noise Abatement Procedures," *11th AIAA/CEAS Aeroacoustics Conference*, AIAA Paper 2005-2981, May 2005.

[46] Merino-Martinez, R., Bertsch, L., Simons, D. G., and Snellen, M., "Analysis of Landing Gear Noise During Approach," *22nd AIAA/CEAS Aeroacoustics Conference*, AIAA Paper 2016-2769, 2016.

[47] Park, S. G., and Clarke, J. P., "Optimal Control Based Vertical Trajectory Determination for Continuous Descent Arrival Procedures," *Journal of Aircraft*, Vol. 52, No. 5, 2015, pp. 1469–1480. doi:10.2514/1.C032967

[48] Park, S. G., and Clarke, J. P., "Vertical Trajectory Optimization to Minimize Environmental Impact in the Presence of Wind," *Journal of Aircraft*, Vol. 53, No. 3, 2016, pp. 725–737. doi:10.2514/1.C032974